analytical chemistry

Article

pubs.acs.org/ac

In Situ TEM and Energy Dispersion Spectrometer Analysis of Chemical Composition Change in ZnO Nanowire Resistive Memories

Yu-Ting Huang,[†] Shih-Ying Yu,[†] Cheng-Lun Hsin,[†,‡] Chun-Wei Huang,[†] Chen-Fang Kang,[§] Fu-Hsuan Chu,[†] Jui-Yuan Chen,[†] Jung-Chih Hu,[⊥] Lien-Tai Chen,[⊥] Jr-Hau He,[§] and Wen-Wei Wu*[,†]

[†]Department of Materials Science and Engineering, National Chiao Tung University, Number 1001, University Road, Hsinchu, Taiwan 30010, R.O.C.

[‡]Department of Electrical Engineering, National Central University, Number 300, Jhongda Road, Jhongli, Taoyuan, Taiwan 32001, R.O.C.

[§]Institute of Photonics and Optoelectronics, National Taiwan University, Number 1, Sec. 4, Roosevelt Road, Taipei, Taiwan 10617, R.O.C.

[⊥]Nanotechnology Research Center, Industrial Technology Institute (ITRI), Chutung, Hsinchu, Taiwan 31040, R.O.C.

Supporting Information

ABSTRACT: Resistive random-access memory (ReRAM) has been of wide interest for its potential to replace flash memory in the next-generation nonvolatile memory roadmap. In this study, we have fabricated the Au/ZnO-nanowire/Au nanomemory device by electron beam lithography and, subsequently, utilized in situ transmission electron microscopy (TEM) to observe the atomic structure evolution from the initial state to the low-resistance state (LRS) in the ZnO nanowire. The element mapping of LRS showing that the nanowire was zinc dominant indicating that the oxygen vacancies were introduced after resistance switching. The results provided direct evidence, suggesting that the resistance change resulted from oxygen migration.

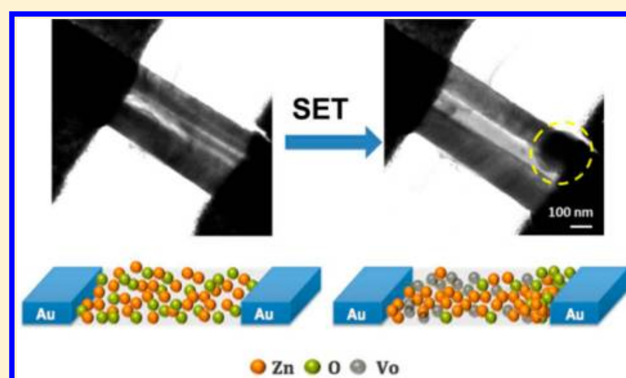

Nowadays, flash memory and dynamic random access memory (DRAM) play the important roles in the contemporary technologies, which are the memories units for cell phones, digital cameras, computers, and so on. The integrated circuit industries are still following the Moore's law, but these two memories have been replaced because of the scaling limit.[1] New technologies have been proposed for the next generation memories. Among them, the resistive random access memory (ReRAM), a nonvolatile memory, is one of the most promising candidates among phase change RAM (PCRAM), ferroelectric RAM (FeRAM), and magnetic RAM (MRAM). It has advantages, including high density, high speed, promising scalability, structural simplicity, less energy consumption, and excellent memory characteristics. The switching times can be 10 ns and the cycling endurances can be up to 10^{12} times.[2−6] Because of these edges/characteristics, ReRAM has the potential to replace the flash memory and DRAM.

The structure of ReRAM is metal/insulator/metal (MIM), which is simple and similar to capacitor. In general, Pt and Au were usually used as contact in ReRAM, and insulator layer could be TiO_2,[7−12] NiO,[13] CoO,[14,15] ZnO,[6,16−21] etc. The filamentary model[1,5,7,14,22−28] and conducting-path-model[9,12,29] are generally accepted by many reports. Filamentary model is based on the conduction in the dielectric matrix/insulator layer,[20,22,30] while conduction path is formed by oxygen ions migration in the conducting-path-model. In FORMING process, the high electric field initially applied to a dielectric layer that can lead the hot spot generation easily to form the conductive filament. If the insulator was an oxide-based material, after applying the bias, the conducting species/oxygen ions would migrate from the cathode to the anode. Oxygen vacancies would be dominant to form the conducting path, then reach the low resistance state (LRS), which was called "SET". After that, the oxygen ions would be restricted and close to the anode. Under bipolar operation and opposite bias, the oxygen ions would travel in the opposite way and combine with the oxygen vacancies to reach the high resistance state (HRS). Likewise, under unipolar operation, the filaments would rupture while the current was drastically increased and provided the Joule heating, and then the LRS would switch to HRS, which was called "RESET".[31] To demonstrate the mechanism of resistive switching, many studies have used different methods to prove this model.[7,11,13−15,23,32−34] However, the mechanism of ReRAM is still not thoroughly understood. For this purpose, we utilized in situ transmission electron microscopy (TEM) to observe the evolution. Additionally, we have used in situ TEM technique to study the kinetics with fruitful results.[35−40]

Received: December 5, 2012
Accepted: March 5, 2013
Published: March 5, 2013

ACS Publications © 2013 American Chemical Society

In this paper, evidence of the resistive switching mechanism were reported. ZnO nanowire-based ReRAM (ZnO-ReRAM) has been fabricated by photolithography and e-beam lithography. We set ZnO-ReRAM to the LRS and studied the structural evolution to observe the filament formed at the LRS. The content of oxygen in the nanowire was decreased while the oxygen elements in the nanowire were extracted near the electrode. A zinc dominant section was evident in the ZnO nanowire, connecting the electrode and being alongside the oxygen dominant counterpart.

■ EXPERIMENTAL SECTION

ZnO nanowires were synthesized in a furnace by the vapor−liquid−solid method.[41,42] One gram of zinc powder and 0.5 g of graphite powder were placed at upstream of the gas flow in the furnace and the Au-coated (100) silicon substrate was placed at downstream near the exhaust of the furnace, and the temperatures were held at 950 and 750 °C, respectively. The vacuum of the system was kept at 0.75 Torr, while argon and oxygen were flown at 100 and 10 sccm, respectively. After the growth process, ZnO nanowires were grown on the substrates.

A 30 nm SiO_2 and a 60 nm Si_3N_4 layers were deposited on the Si substrate by low pressure chemical vapor deposition system front and back. After the positive photoresist (PR, FH6400, from Fujifilm Olin) was coated and baked at 90 °C for 1 min, the region at the bottom window was defined by photolithography. Then the SiO_2 and Si_3N_4 layer were removed by reactive ion etching (RIE) to expose the Si at bottom window, followed by 20% KOH solution dipping at 85 °C for 2.5 h, leaving a Si_3N_4 layer as a TEM observation window.[43] Photolithography was used to define the main electrodes. A 20 nm Ti and a 40 nm Au were deposited by electron gun evaporation system as the contact metal. After deposition process, the PR was removed by acetone. ZnO nanowires were dispersed in alcohol and then dropped on the substrate until nanowires were placed inside the window region for TEM observation. Methyl methacrylate (bottom layer) and polymethyl methacrylate (top layer) were coated as positive tone photoresists (manufactured by Micro Chem), followed by 180 °C baking for 1 min. E-beam was used to make the contact with 2−10 min exposure time. After developing the exposed area by e-beam, a 30 nm Ti and a 120 nm Au were deposited as the electrodes by electron gun deposition system. After deposition, the PR was removed by lift-off process in acetone. The photolithography and e-beam lithography process of the ZnO-ReRAM were shown in Figure 1a and b, respectively. The corresponding scanning electron microscopy (SEM) images of the device were shown in Supporting Information Figure S-1. The microstructure was inspected by SEM and TEM. In situ TEM observations were carried out in JEOL 2000 V ultra high vacuum-TEM, which was equipped with a video recorder with 1/30 s time resolution. Energy dispersive X-ray spectroscopy (EDS) equipped with JEOL 2100F TEM was used to investigate the chemical composition difference of the nanowire between the initial state and LRS. The switching behavior was operated by Keithley 4200.

■ RESULTS AND DISCUSSION

The diameter and the length of the nanowire were of 100 nm and 5 μm, respectively, as shown in Figure 2a. Figure 2b is the TEM image of the ZnO nanowire, and Figure 2c is the corresponding high resolution transmission electron microscopy (HRTEM) image. The inset in Figure 2c is the diffraction pattern. The growth direction of the single crystalline nanowire is [0001].

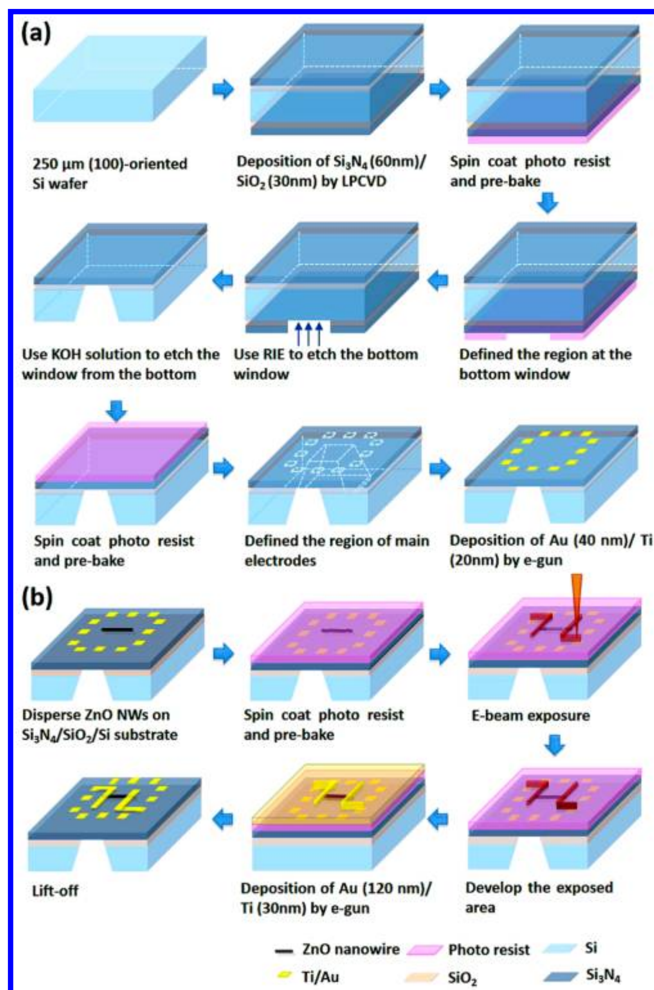

Figure 1. Schematic illustration of the sample fabrication process of ZnO-ReRAM. (a) Photolithography process. (b) E-beam lithography process.

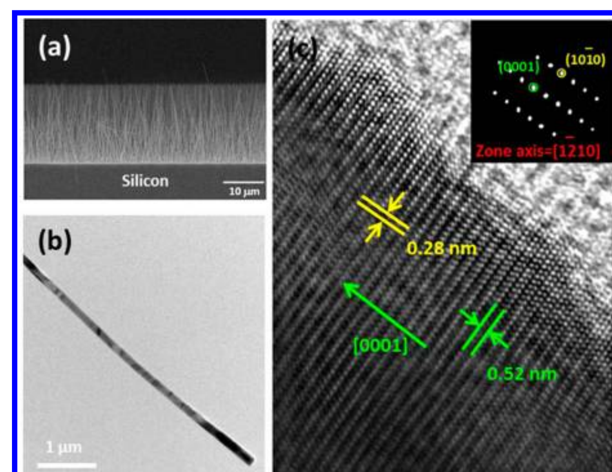

Figure 2. (a) SEM image of as-grown ZnO nanowires on Si substrate. (b) TEM image of single ZnO nanowire with 5 μm in length and 100 nm in diameter. (c) High-resolution transmission electron microscopy (HRTEM) image of ZnO nanowire with [0001] growth direction. The insert shows the corresponding electron diffraction pattern with [$1\bar{2}10$] zone axis.

dx.doi.org/10.1021/ac303528m | Anal. Chem. 2013, 85, 3955−3960

Figure 3 shows a series of ZnO-ReRAM of in situ TEM images clipped from the video. The contact electrode at the left is the cathode while the right one is the anode. After applied a positive bias (3 V), the sequence of the SET process was shown in Figure 3b–d. While the device turned from HRS to LRS, the protrusion as-formed near the anode was shown in Figure 3d. The detail of electrical properties was shown in Supporting Information Figure S-2. To analyze the elements and confirm the phenomenon, we fabricated another device (Figure 4) for conventional TEM holder and found out the nanowire on this device has the same behavior with device in Figure 3.

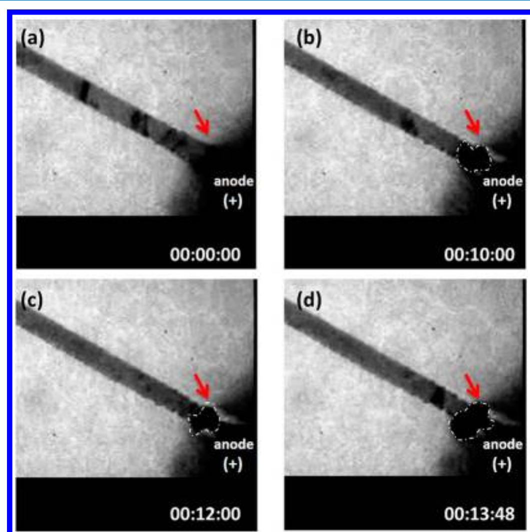

Figure 3. Series of in situ TEM images clipped from the video. (a) The initial state of ZnO nanowire. (b and c) The sequence of the SET process. (d) The ZnO nanowire of LRS state with the as-formed protrusion near the anode. The contact electrode at the left is the cathode while the right one is the anode. The red arrow pointed at the occurrence of the protrusion.

The ZnO-ReRAM with 500 nm electrode spacing was shown in Figure 4a. In this case, the ZnO-ReRAM contains two nanowires. The electrode spacing is an important parameter. If the spacing is too large (>1 mm), the resistive switching behavior could not be obtained.[18]

The typical electrical property ($I-V$ curve) of the device was shown in Figure 4e. The bottom electrode was defined as anode while the top electrode was the grounded electrode or cathode. First, positive bias was applied at the bottom electrode for the FORMING of the device. Next, positive bias was applied again to induce the defect-induced soft breakdown while the current increased suddenly. At the beginning of the RESET process, the current would reach the limit at the low resistance state. After the resistive switching, the memristive effect of the ZnO-ReRAM was confirmed. Then the device was manually held at LRS state, which is a purple line of Figure 4e, and the morphology/structure of the ZnO-ReRAM was inspected by TEM to observe the evolution of the ZnO nanowire.

Figure 4b shows the corresponding TEM image of the ZnO-ReRAM at the low resistive state. The yellow-dashed circle near the anode highlighted the evolution of the nanowire. The morphology of the nanowire at the anode changed, which indicated that there was anions migration and only oxygen ions were the anions in the ZnO nanowire. It is presumable that the highlighted region was due to the oxygen ion migration from the cathode to the anode, and then oxygen ions were restricted to the electrode.[8,10,44,45] This phenomenon would contributed to the generation of oxygen vacancies in the nanowire and turn it to be zinc dominant. This result supports the unipolar operation of filament model, and shows the evolution of nanowire structure/morphology.

According to the EDS spectrum and the elemental mapping confirming the element of the extra area, we discuss the mechanism of our ZnO nanowire-based resistivity switching device as follows.

The EDS of the ZnO nanowire at the red points in Figure 4a and b was shown in Figure 4c and d, respectively. In these two figures, only zinc and oxygen element were depicted with the removal of Si signals for exquisite comparison and calculation. In Figure 4c, the atomic ratio of zinc and oxygen was nearly 1:1 before the resistive switching. After resistive switching, the ratio of zinc and oxygen turns to 3:1 (Figure 4d) with the standard deviation of 2.9% (Supporting Information Table S-1). The change of the chemical composition ratio of the nanowire was an evidence to prove that the switching process from HRS to LRS was due to the oxygen ion migration, resulting in dramatic reduction of the oxygen ratio and zinc majority at the SET state. The O/Zn ratio of HRS state was lower than LRS state at highlighted region and higher than LRS state at red point in Figure 4b, which suggested that the partial oxygen ions were from the anode and the recombination with oxygen vacancies could break the conducting filament (Supporting Information Figure S-3). The upper electrode is cathode and the lower one is anode. After application of the positive voltage on the device to switch from HRS to LRS during the SET process, the protrusion occurred near the anode pointed with the red arrow. This result illustrated that the partial oxygen ions were moving toward to anode and restricted in/near the electrode. This result is consistent with the one in Figure 4b and the presumption mentioned in the introduction.

Figure 5b and c are the EDS mapping of oxygen and zinc element, respectively in the highlighted region in Figure 4b. Figure 5a is the corresponding TEM image of Figure 5b and c. In Figure 5, we tilted an angle for the sample relative to Figure 4 to avoid confusion of element distribution from the EDS overlap of the extra area and ZnO nanowire. The oxygen distribution illustrated that oxygen with high concentration was restricted at the anode, analogous to the result in Figure 4 that the ZnO nanowire has changed to zinc dominant nanowire. The EDS analysis of the highlighted region also shows the O/Zn ratio is higher than red point in Figure 4b (Supporting Information Figure S-4). The reaction has been presumed in two steps as follows:

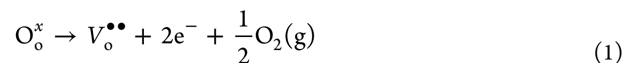

$$\mathrm{O}_\mathrm{o}^x \rightarrow V_\mathrm{o}^{\bullet\bullet} + 2\mathrm{e}^- + \frac{1}{2}\mathrm{O}_2(\mathrm{g}) \tag{1}$$

$$\frac{1}{2}\mathrm{O}_2(\mathrm{g}) \rightarrow \mathrm{O}^{2-} + 2h^+ \tag{2}$$

For the net reaction

$$\mathrm{O}_\mathrm{o}^x \rightarrow V_\mathrm{o}'' + \mathrm{O}^{2-} \tag{3}$$

The oxygen was decomposed into oxygen vacancies and oxygen ions and deformed the nanowire, leaving oxygen vacancies to be the dominant in the nanowire.[17,21,46] Our results prove that the conducting paths were formed by oxygen ion migration from HRS to LRS during the SET process. The mechanism of the resistive switching of the ZnO-ReRAM could be illustrated in Figure 6. During the forming process, the electric field near the

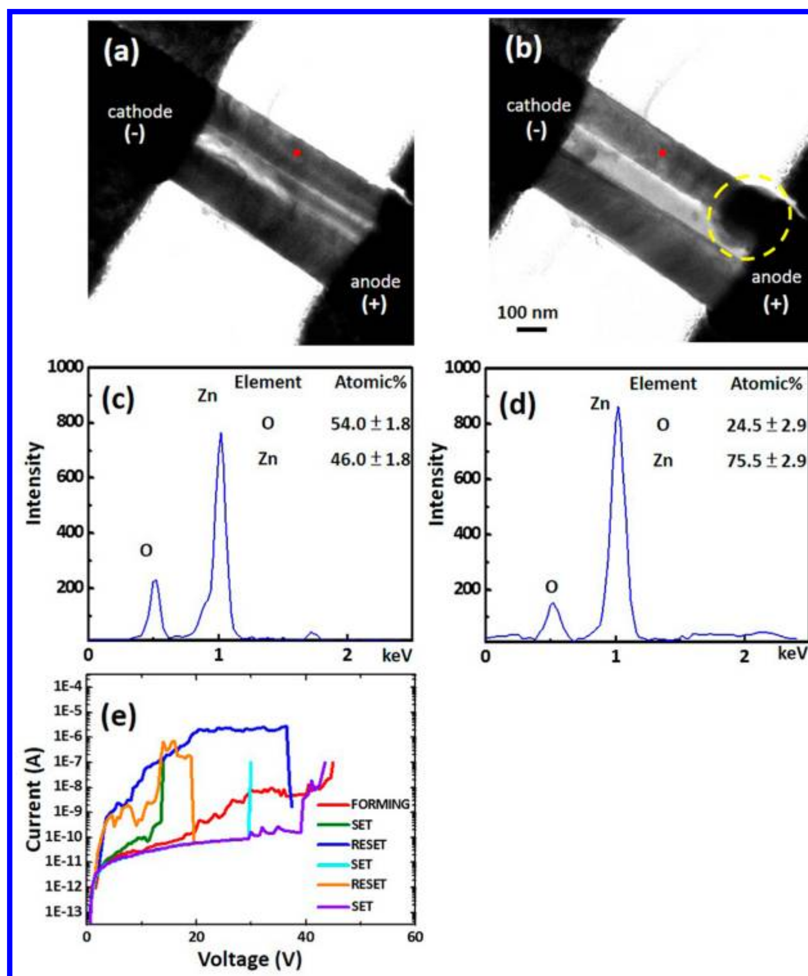

Figure 4. TEM image of the ZnO-ReRAM (a) before and (b) after the resistive switching. The yellow-dashed circle near the anode in (b) highlighted the evolution of the nanowire. Panels c and d were the EDS spectra of the red dots in panels a and b, respectively. The inset in each spectrum shows the corresponding atomic ratio of zinc and oxygen. (e) The typical current−voltage curve measured by voltage sweep to form and SET/RESET the ZnO-ReRAM device.

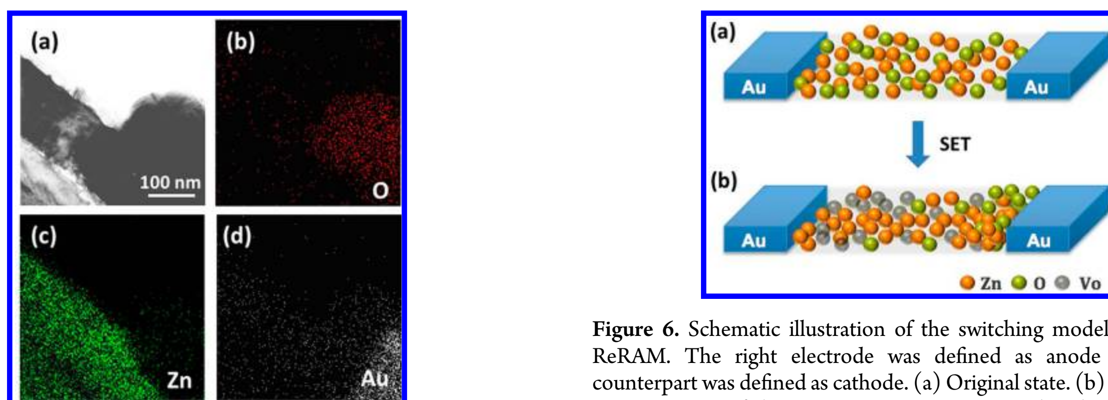

Figure 5. EDS mapping diagrams. (a) The corresponding TEM image of the ZnO nanowire. Panels b, c, and d were EDS element mapping diagrams of oxygen, zinc and gold, respectively in the ZnO nanowire at low resistance state. The sample had been tilt for observed more clearly. At the low resistance state, the oxygen ions were mainly near the anode, while the zinc ions and oxygen vacancies formed the conducting path.

Figure 6. Schematic illustration of the switching model of the ZnO-ReRAM. The right electrode was defined as anode and the left counterpart was defined as cathode. (a) Original state. (b) After the SET process. Most of the oxygen ions were restricted and gathered at the anode, while the zinc ions and oxygen vacancies formed the conducting path.

electrode was higher than that in space-charge region, and the soft breakdown would occur at the interface region.[16] When we applied the positive bias again, the space-charge region would break down as eq 3, and the oxygen ions would have the potential to migrate to the anode and restricted alongside the electrode. Meanwhile, the oxygen vacancies would form the conducting path (from Figure 6a to 6b, the SET process).[14,19,24,25,47−49] The model of the unipolar switching mechanism was confirmed directly by the EDS results. From this model, we could know the true mechanism in our memristive switching is the migration of oxygen. Because of the unipolar operation, the polarity of the bias was not changed. The positive bias applied could increase the

current and provide the Joule heating to break the as-formed conducting filament, resulting in the removal of oxygen ions from the anode and the recombination with oxygen vacancies.[16,17,26,31] After the rupture of the filament, the resistance would turn back to HRS. Our observation provides evidence on the role of oxygen to form the conducting path in the matrix. Furthermore, the electrode should have the ability to restrict the oxygen ions; otherwise, the device would have had poor retention and even failed at the RESET process.[50]

■ CONCLUSIONS

In conclusion, we have fabricated the ZnO nanowire based memristive device. We observed the structure evolution of the ZnO nanowire and inspected the chemical composition by the EDS spectrum and element mapping after the resistance switched to the LRS. The results proved that the zinc/oxygen ratio of the ZnO nanowire would increase for the oxygen migration to/near the anode. This study demonstrated that the SET process was due to the migration of oxygen ions. Our results identify the mechanism of the switching behavior and would have significant influence on the device fabrication, materials design, and applications of ReRAM in the future technologies.

■ ASSOCIATED CONTENT

Supporting Information

In situ TEM video presenting the dynamic observation of the ZnO-ReRAM from HRS to LRS during the SET process and additional figures as described in the text. This material is available free of charge via the Internet at http://pubs.acs.org.

■ AUTHOR INFORMATION

Corresponding Author

*E-mail: WWWu@mail.nctu.edu.tw.

Notes

The authors declare no competing financial interest.

■ ACKNOWLEDGMENTS

We acknowledge the support by National Science Council through grants 100-2628-E-009-023-MY3 and 99-2120-M-007-011

■ REFERENCES

(1) Waser, R.; Aono, M. *Nat. Mater.* **2007**, *6*, 833−840.
(2) Meister, S.; Kim, S.; Cha, J. J.; Wong, H. S. P.; Cui, Y. *ACS Nano* **2011**, *5*, 2742−2748.
(3) Meister, S.; Schoen, D. T.; Topinka, M. A.; Minor, A. M.; Cui, Y. *Nano Lett.* **2008**, *8*, 4562−4567.
(4) Jo, S. H.; Kim, K. H.; Lu, W. *Nano Lett.* **2009**, *9*, 870−874.
(5) Lee, M. J.; Lee, C. B.; Lee, D.; Lee, S. R.; Chang, M.; Hur, J. H.; Kim, Y. B.; Kim, C. J.; Seo, D. H.; Seo, S.; Chung, U. I.; Yoo, I. K.; Kim, K. *Nat. Mater.* **2011**, *10*, 625−630.
(6) Sohn, J. I.; Choi, S. S.; Morris, S. M.; Bendall, J. S.; Coles, H. J.; Hong, W. K.; Jo, G.; Lee, T.; Welland, M. E. *Nano Lett.* **2010**, *10*, 4316−4320.
(7) Kim, M.; Kwon, D. H.; Kim, K. M.; Jang, J. H.; Jeon, J. M.; Lee, M. H.; Kim, G. H.; Li, X. S.; Park, G. S.; Lee, B.; Han, S.; Hwang, C. S. *Nat. Nanotechnol.* **2010**, *5*, 148−153.
(8) Jeong, D. S.; Schroeder, H.; Breuer, U.; Waser, R. *J. Appl. Phys.* **2008**, *104*, 123716.
(9) Yoshida, C.; Tsunoda, K.; Noshiro, H.; Sugiyama, Y. *Appl. Phys. Lett.* **2007**, *91*, 223510.
(10) Jeong, H. Y.; Lee, J. Y.; Choi, S. Y. *Adv. Funct. Mater.* **2010**, *20*, 3912−3917.
(11) Park, B. H.; Yoon, I. S.; Choi, J. S.; Kim, Y. S.; Hong, S. H.; Hwang, I. R.; Park, Y. C.; Kang, S. O.; Kim, J. S. *Appl. Phys. Express* **2011**, *4*, 041101.
(12) Choi, B. J.; Jeong, D. S.; Kim, S. K.; Rohde, C.; Choi, S.; Oh, J. H.; Kim, H. J.; Hwang, C. S.; Szot, K.; Waser, R.; Reichenberg, B.; Tiedke, S. *J. Appl. Phys.* **2005**, *98*, 033715.
(13) Yanagida, T.; Oka, K.; Nagashima, K.; Kawai, T.; Kim, J. S.; Park, B. H. *J. Am. Chem. Soc.* **2010**, *132*, 6634−6635.
(14) Yanagida, T.; Nagashima, K.; Oka, K.; Kanai, M.; Klamchuen, A.; Kim, J. S.; Park, B. H.; Kawai, T. *Nano Lett.* **2011**, *11*, 2114−2118.
(15) Yanagida, T.; Nagashima, K.; Oka, K.; Taniguchi, M.; Kawai, T.; Kim, J. S.; Park, B. H. *Nano Lett.* **2010**, *10*, 1359−1363.
(16) Xu, N.; Liu, L. F.; Sun, X.; Liu, X. Y.; Han, D. D.; Wang, Y.; Han, R. Q.; Kang, J. F.; Yu, B. *Appl. Phys. Lett.* **2008**, *92*, 232112.
(17) Yoon, J.; Hong, W. K.; Jo, M.; Jo, G.; Choe, M.; Park, W.; Sohn, J. I.; Nedic, S.; Hwang, H.; Welland, M. E.; Lee, T. *ACS Nano* **2011**, *5*, 558−64.
(18) Gao, M.; Yang, Y. C.; Zhang, X. X.; Zeng, F.; Zhou, W. Y.; Xie, S. S.; Pan, F. *Nanoscale* **2011**, *3*, 1917−1921.
(19) Chang, W. Y.; Peng, C. S.; Lin, C. H.; Tsai, J. M.; Chiu, F. C.; Chueh, Y. L. *J. Electrochem. Soc.* **2011**, *158*, H872−H875.
(20) Chang, W. Y.; Lin, C. A.; He, J. H.; Wu, T. B. *Appl. Phys. Lett.* **2010**, *96*, 242109.
(21) Ke, J. J.; Liu, Z. J.; Kang, C. F.; Lin, S. J.; He, J. H. *Appl. Phys. Lett.* **2011**, *99*, 192106.
(22) Kim, K. M.; Song, S. J.; Kim, G. H.; Seok, J. Y.; Lee, M. H.; Yoon, J. H.; Park, J.; Hwang, C. S. *Adv. Funct. Mater.* **2011**, *21*, 1587−1592.
(23) Lee, M. J.; Han, S.; Jeon, S. H.; Park, B. H.; Kang, B. S.; Ahn, S. E.; Kim, K. H.; Lee, C. B.; Kim, C. J.; Yoo, I. K.; Seo, D. H.; Li, X. S.; Park, J. B.; Lee, J. H.; Park, Y. *Nano Lett.* **2009**, *9*, 1476−1481.
(24) Liu, Q.; Long, S. B.; Lv, H. B.; Wang, W.; Niu, J. B.; Huo, Z. L.; Chen, J. N.; Liu, M. *Acs Nano* **2010**, *4*, 6162−6168.
(25) Hong, S. S.; Cha, J. J.; Cui, Y. *Nano Lett.* **2011**, *11*, 231−235.
(26) Yao, J.; Sun, Z. Z.; Zhong, L.; Natelson, D.; Tour, J. M. *Nano Lett.* **2010**, *10*, 4105−4110.
(27) Hsiung, C. P.; Liao, H. W.; Gan, J. Y.; Wu, T. B.; Hwang, J. C.; Chen, F.; Tsai, M. J. *ACS Nano* **2010**, *4*, 5414−5420.
(28) Qi, J.; Olmedo, M.; Ren, J. J.; Zhan, N.; Zhao, J. Z.; Zheng, J. G.; Liu, J. L. *ACS Nano* **2012**, *6*, 1051−1058.
(29) Rozenberg, M. J.; Inoue, I. H.; Sanchez, M. J. *Phys. Rev. Lett.* **2004**, *92*, 178302.
(30) Lee, M. J.; Park, Y.; Suh, D. S.; Lee, E. H.; Seo, S.; Kim, D. C.; Jung, R.; Kang, B. S.; Ahn, S. E.; Lee, C. B.; Seo, D. H.; Cha, Y. K.; Yoo, I. K.; Kim, J. S.; Park, B. H. *Adv. Mater.* **2007**, *19*, 3919−3923.
(31) Sawa, A. *Mater. Today* **2008**, *11*, 28−36.
(32) Fujimoto, M.; Koyama, H.; Konagai, M.; Hosoi, Y.; Ishihara, K.; Ohnishi, S.; Awaya, N. *Appl. Phys. Lett.* **2006**, *89*, 223509.
(33) Yasuhara, R.; Fujiwara, K.; Horiba, K.; Kumigashira, H.; Kotsugi, M.; Oshima, M.; Takagi, H. *Appl. Phys. Lett.* **2009**, *95*, 012110.
(34) Mizukami, T.; Miyato, Y.; Kobayashi, K.; Matsushige, K.; Yamada, H. *Appl. Phys. Lett.* **2011**, *98*, 083120.
(35) Chen, K. C.; Wu, W. W.; Liao, C. N.; Chen, L. J.; Tu, K. N. *Science* **2008**, *321*, 1066−1069.
(36) Lu, K. C.; Wu, W. W.; Ouyang, H.; Lin, Y. C.; Huang, Y.; Wang, C. W.; Wu, Z. W.; Huang, C. W.; Chen, L. J.; Tu, K. N. *Nano Lett.* **2011**, *11*, 2753−2758.
(37) Chou, Y. C.; Wu, W. W.; Chen, L. J.; Tu, K. N. *Nano Lett.* **2009**, *9*, 2337−2342.
(38) Chen, L. J.; Wu, W. W. *Mater. Sci. Eng. R* **2010**, *70*, 303−319.
(39) Hsin, C. L.; Lee, W. F.; Huang, C. T.; Huang, C. W.; Wu, W. W.; Chen, L. J. *Nano Lett.* **2011**, *11*, 4348−4351.
(40) Wu, W. W.; Lu, K. C.; Wang, C. W.; Hsieh, H. Y.; Chen, S. Y.; Chou, Y. C.; Yu, S. Y.; Chen, L. J.; Tu, K. N. *Nano Lett.* **2010**, *10*, 3984−3989.
(41) Chu, F. H.; Huang, C. W.; Hsin, C. L.; Wang, C. W.; Yu, S. Y.; Yeh, P. H.; Wu, W. W. *Nanoscale* **2012**, *4*, 1471−1475.
(42) Meister, S.; Peng, H. L.; McIlwrath, K.; Jarausch, K.; Zhang, X. F.; Cui, Y. *Nano Lett.* **2006**, *6*, 1514−1517.

(43) Seidel, H.; Csepregi, L.; Heuberger, A.; Baumgartel, H. *J. Electrochem. Soc.* **1990**, *137*, 3612−3626.
(44) Waser, R.; Dittmann, R.; Staikov, G.; Szot, K. *Adv. Mater.* **2009**, *21*, 2632−2663.
(45) Goux, L.; Czarnecki, P.; Chen, Y. Y.; Pantisano, L.; Wang, X. P.; Degraeve, R.; Govoreanu, B.; Jurczak, M.; Wouters, D. J.; Altimime, L. *Appl. Phys. Lett.* **2010**, *97*, 243509.
(46) Hsu, C.-W.; Chou, L.-J. *Nano Lett.* **2012**, *12*, 4247−4253.
(47) Szot, K.; Speier, W.; Bihlmayer, G.; Waser, R. *Nat. Mater.* **2006**, *5*, 312−320.
(48) Joshua Yang, J.; Miao, F.; Pickett, M. D.; Ohlberg, D. A.; Stewart, D. R.; Lau, C. N.; Williams, R. S. *Nanotechnology* **2009**, *20*, 215201.
(49) Goux, L.; Chen, Y. Y.; Pantisano, L.; Wang, X. P.; Groeseneken, G.; Jurczak, M.; Wouters, D. J. *Electrochem. Solid State Lett.* **2010**, *13*, G54−G56.
(50) Gao, B.; Kang, J. F.; Liu, L. F.; Liu, X. Y.; Yu, B. *Appl. Phys. Lett.* **2011**, *98*, 232108.